Influence of Martensitic Structure and Carbide Precipitation Behavior on Mechanical Properties of 25CrMoNbB Alloy Steels with Mo Contents of 0.25 and 0.5 Pct

YAXU ZHENG, FUMING WANG, WARREN M. GARRISON Jr., YU LIN, and CHANGRONG LI

In this article, the effects of Mo contents of 0.25 and 0.50 pct on the martensitic structure and carbide precipitation behavior of the experimental steels were investigated and their effects on strength, toughness, and fatigue strength were studied. The results showed that the martensitic blocks and laths were refined and the dislocation density increased with the addition of Mo contents of 0.25 and 0.50 pct. Meanwhile, the amount of carbides increased and the size of carbides decreased in tempered steels. The refinement of carbides is due to the increment of nucleation sites resulting from martensitic structure refinement and the dislocation density increment. Besides, the improvement of thermal stability of $M_{23}C_6$ carbides enriched with Mo also contributes to carbide refinement. With the addition of 0.50 pct Mo, the strength was improved and the toughness did not deteriorate compared with the steel 0.25 pct Mo. Meanwhile, the fatigue strength was also significantly improved with the addition of 0.50 pct Mo.

I. INTRODUCTION

IN recent years, the use of high-speed trains has developed rapidly in China. With train speeds above 350 km/h, the hardenability and mechanical properties of larger diameter train axles need to be improved. However, the improvement of tensile strength is usually accompanied with the deterioration of impact toughness.[1] It is necessary to develop material that exhibits both high strength and good toughness to satisfy the requirement of safety of train axles. Now, the hardenability of large size axles produced by some Chinese steel companies is not good enough and there is a great amount of large size ferrite in axles, which reduces strength significantly.

It was reported that a small amount of Mo in steel could improve hardenability and delay ferrite formation.[2] Besides, Mo has influence on carbide precipitation behavior. Lee et al.[3] reported that Mo enhanced the effect of precipitation hardening in HSLA steels containing Nb. Previous research results[4–9] indicated that Mo significantly reduced the size of the carbides and strongly retarded their coarsening during heat treatment. This was because it enhanced the nucleation rate by reducing the interfacial energy. The addition of Mo promotes nucleation of MC-type carbides such as (Ti, Mo)C, (Nb, Mo)C, and (V, Mo)C. It is easy to form precipitates with diameters less than 20 nm, since Mo could reduce interfacial energy and Gibbs free energy for precipitation. The carbides with more Mo fraction have good thermal stability. Therefore, they are not easy to coarsen.[10–12] Wieczerzak et al.[13] reported that the thermal stability of $M_{23}C_6$ carbides at higher temperatures was improved by the addition of Mo in Fe-25Cr-0.8C heat-resistant steel, since the Cr and Fe atoms in $M_{23}C_6$ carbides can be replaced by Mo.

Mo is beneficial for reducing temper embrittlement of quenched and tempered steels, especially for large size structural components. Normally, Mo content is less than 0.7 wt pct in structural steels to avoid temper embrittlement. Wada and Hagel[14] studied the effect of Mo content on temper embrittlement of 2.25 Cr-1Mo steel and found that the fracture appearance transition

YAXU ZHENG and FUMING WANG are with the School of Metallurgical and Ecological Engineering, University of Science and Technology Beijing, No. 30, Xueyuan Road, Haidian District, Beijing 100083, P.R. China. Contact email: wangfuming@metall.ustb.edu.cn WARREN M. GARRISON, Jr. and YU LIN are with the Materials Science and Engineering Department, Carnegie Mellon University, Pittsburgh PA 15213. CHANGRONG LI is with the School of Materials Science and Engineering, University of Science and Technology Beijing, Beijing 100083, P.R. China.

temperature (FATT) was the lowest when Mo content was about 0.50 pct. Mo can refine the carbide precipitates and delay the coarsening of martensitic lath during tempering.

In order to improve hardenability and strength of axle steel, Mo was added to the experimental steels. There are few systematical studies about the effect of Mo on refining martensitic microstructure and the effects of martensitic structure and dislocation density on carbide precipitation behavior in tempered steel. In this article, the effects of Mo on martensitic effective grain size and lath width were studied. At the same time, the dislocation density in the experimental steels was also measured with the help of X-ray diffraction (XRD). The equilibrium precipitates in the studied steels were calculated by use of Thermo-Calc (Thermo-Calc Software Company, Sweden). The carbides in the tempered steels were analyzed by use of transmission electron microscopy (TEM). The aim of this article is to study the effects of Mo contents of 0.25 and 0.50 pct on refining martensitic microstructure and carbide precipitates and the effects of martensitic structure and dislocation density on carbide precipitation behavior in the tempered steels. Finally, the comprehensive effects of martensitic structure and carbide precipitates on mechanical properties, including tensile strength, toughness, and fatigue strength, will also be discussed.

II. EXPERIMENTAL

A. Materials and Heat Treatment Processes

The chemical compositions of the investigated steels are given in Table I. The 50-kg vacuum induction furnace was used to produce the experimental steels. The diameters of two ends of ingot were 150 and 100 mm, respectively. The length of the ingot was 350 mm. First, the ingots were heated at 1473 K (1200 °C) for 10 hours to homogenize the alloying elements. Then, they were forged into steel bars with a diameter of 16 mm with a strain rate of about 0.5 s^{-1}. The start temperature of forging was 1423 K (1150 °C), and the final temperature of forging was 1123 K to 1173 K (850 °C to 900 °C). The steel bars were air cooled after forging. The microstructures of steel 0.5 pct Mo before heat treatment are ferrite, martensite, and granular bainite, as shown in Figure 1. The schematic illustration of the heat treatment procedures is shown in Figure 2. First, the steel bars were heated at 1193 K (920 °C) for 0.5 hours to homogenize the microstructure. Then, they were austenitized at 1173 K (900 °C) for 1 hour and quenched in water. Finally, they were tempered at 903 K (630 °C) for 1 hour.

B. Microstructure and Precipitate Characterization

The quenched specimens were etched with supersaturated picric acid and sodium dodecyl benzene sulfonate aqueous solution at 338 K (65 °C) for 2 minutes after mechanical polishing for observation of prior austenite grains (PAGs) by optical microscopy (OM, LJ-JX2030).[15] The crystallographic orientation, average grain size, and misorientation angle distribution of martensite were determined by electron backscattered diffraction (EBSD, JSM-7800 F). The EBSD scanning step was 0.1 μm and the total scanning area was about 100 μm × 100 μm to do statistic measurement of average block size and misorientation angle distribution of martensite. The EBSD specimens were prepared by electropolishing with 5 pct perchloric acid. The martensitic laths were observed using TEM (Tecnai G2 F20

Table I. Chemical Compositions of the Experimental Steels (Weight Percent)

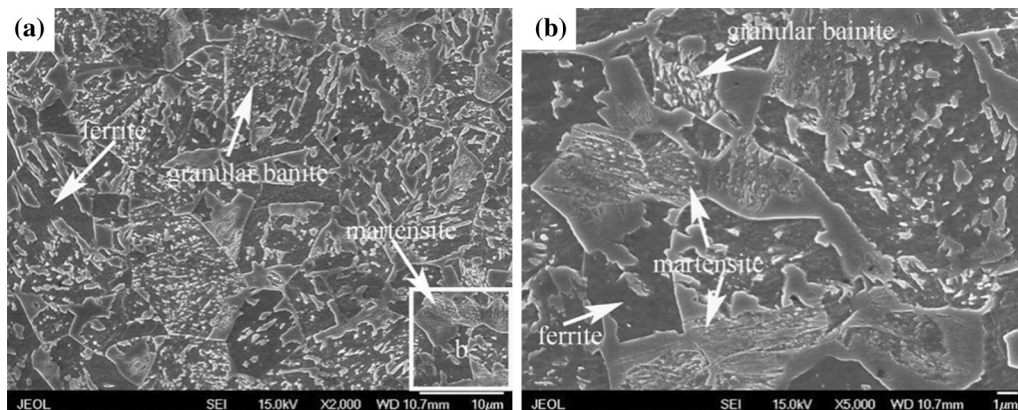| Steel	C	Si	Mn	P	S	Cr	Mo	V	Ni	N	O	Nb	B
1	0.26	0.34	0.71	< 0.010	< 0.005	1.07	—	0.12	0.29	0.0017	0.0015	0.04	0.0018
2	0.27	0.32	0.70	< 0.010	< 0.005	1.08	0.25	0.12	0.30	0.0017	0.0015	0.04	0.0021
3	0.26	0.30	0.71	< 0.010	< 0.005	1.06	0.50	0.12	0.28	0.0020	0.0013	0.04	0.0020

Fig. 1—(a) Overall microstructure and (b) detail microstructure of steel 0.5 pct Mo before heat treatment.

S-TWIN), and almost 100 martensitic laths were counted to calculate the average width. The precipitates in the tempered steel were analyzed by TEM and energy-dispersive spectrometry (EDS, Tecnai G2 F20 S-TWIN).

The thin foils used for TEM observation were twin-jet electropolished with 5 pct perchloric acid. The carbon extraction replicas used for TEM observation were prepared by plating a carbon film with 20- to 30-nm thickness on the sample surface that had been etched with 4 pct nital after being mechanically polished. Then, the carbon films were stripped off with 4 pct nital and collected with copper net.[16] J Mat Pro software (Sente Software Company, England) was used to calculate the continuous cooling transformation (CCT) curves and phase transformation temperatures of the experimental steels. The thermodynamic calculation of equilibrium precipitation for precipitates was carried out with Thermo-Calc software. Image J software (National Institutes of Health Company, USA) was used to measure carbide size and area fraction. The area of each carbide was measured by Image J software and the diameter of each carbide was calculated from the
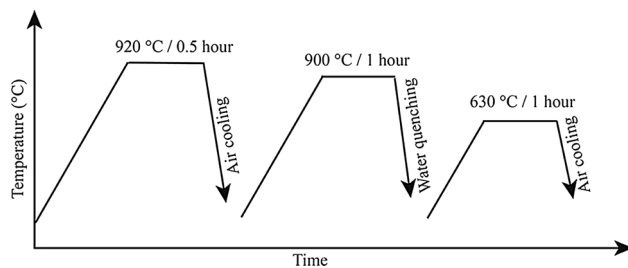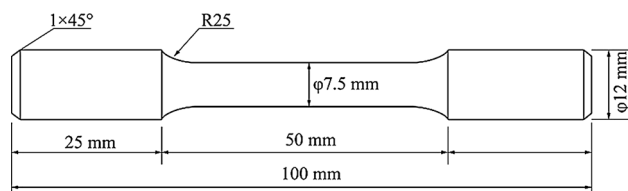
measured area assuming the particles be spherical. The carbides within about 10 μm $\times$ 10 μm area were counted for statistics of size and area fraction. The dislocation density was measured by XRD (PHILIPS APD-10X, PHILIPS, Holland; Cu anode). The voltage, current, and scanning step size were 40 kV, 40 mA, and 0.05 deg, respectively. The scanning area was 15 mm $\times$ 10 mm.

C. Mechanical Properties

The tensile strength and Charpy U-notch impact tests of as-quenched and tempered steels were conducted at room temperature. The tensile test and U-notch Charpy impact test were conducted according to Chinese standards GB/T 228.1-2010 and GB/T 229-2007, respectively. The U-notch Charpy of train axle is required in Europe standard EN13261-2009. U-notch Charpy is usually used to analyze the tendency of crack initiation of material, and V-notch Charpy is usually used to analyze the tendency of crack propagation. For train axle, the fatigue cracks usually initiate on the axle surface. The cracks will propagate quickly with high rotation speed if there are some microcracks on the axle. Therefore, the low tendency of crack initiation of material is important. Five tests were performed for each test condition and the statistical tests of the data were analyzed using the box-plot method. The outliers were removed, and the average of the other data was noted.[16] The fatigue strength and S-N curves were tested by a rotating-bending fatigue testing machine (PQ1-6) according to Chinese standard GB/T 4337-2008. The dimensions of tensile specimens were 5 mm $\times$ 30 mm o.d., and those of Charpy impact specimens were 10 mm $\times$ 10 mm $\times$ 55 mm. The dimensions of the specimen for rotating-bending fatigue testing are shown in Figure 3.

III. RESULTS AND DISCUSSION

A. Effect of Mo Content on Martensitic Microstructure

The typical morphologies of PAGs are shown in Figure 4. The average austenite grain sizes are 7.2 $\pm$ 1.4 μm, 6.9 $\pm$ 1.1 μm, and 7.5 $\pm$ 1.5 μm for steel 0 pct Mo, steel 0.25 pct Mo, and steel 0.5 pct Mo,

Fig. 2—Schematic illustration of the heat treatment procedures.

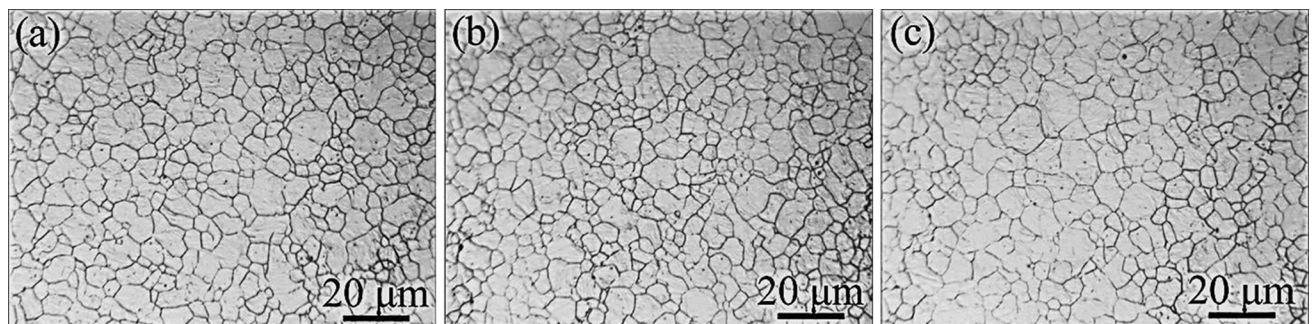Fig. 3—Dimension of specimen for rotating-bending fatigue testing.

Fig. 4—Austenite grain morphologies observed by OM: (a) steel 0 pct Mo, (b) steel 0.25 pct Mo, and (c) steel 0.50 pct Mo.

respectively. There is no obvious difference of PAG size for the three experimental steels.

Normally, one PAG is divided into several martensitic packets. Each packet is further divided into martensitic blocks, and each block is composed of several laths, which are in parallel arrangement.[16] The schematic diagram of martensitic microstructure is shown in Figure 5. The blocks in one packet are separated by high-angle grain boundaries (HAGBs), and the laths in one block are separated by low-angle grain boundaries (LAGBs). For cleavage fracture, the HAGB can effectively prevent the crack propagation and change the propagation direction.[17,18] Block is the minimum unit controlling the toughness and strength of martensite steel. Therefore, the effective grain size is equal to the average size of the blocks.[19–21]

The total EBSD scanning area was about 100 μm × 100 μm for each tested steel to do statistical measurement of block size and misorientation angle distribution of martensite. The crystallographic orientation maps
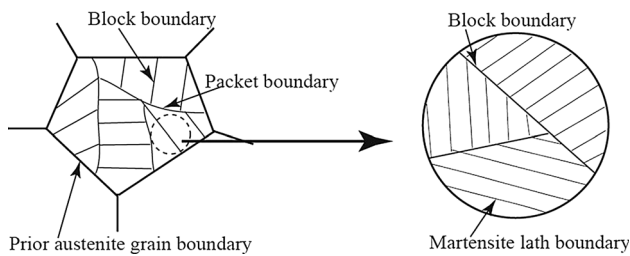

Fig. 5—Schematic diagram of martensite structure.

and block size distribution in the tempered samples analyzed by EBSD are shown in Figure 6. The average effective block sizes, considering a misorientation criteria above 15 deg (HAGB), are 1.353 ± 0.41, 1.054 ± 0.26, and 0.874 ± 0.37 μm for steel 0 pct Mo, steel 0.25 pct Mo, and steel 0.5 pct Mo, respectively.

The HAGBs above 15 deg and LAGBs of 2 to 15 deg are analyzed. The influence of Mo content on block size and HAGB percentage is shown in Figure 7. The percentages of HAGB of steel 0 pct Mo, steel 0.25 pct Mo, and steel 0.5 pct Mo are 30.1 ± 6.3, 35.7 ± 4.5, and 34.2 ± 5.3 pct, respectively. It is easy to discover that martensitic block is refined. However, there is no obvious change of the HAGB percentage with increasing Mo content in steels.

The martensitic microstructure morphologies of the tempered steels analyzed by TEM are shown in Figure 8. Almost 100 martensitic laths were observed and counted to calculate the average width. The results of distribution and average width of martensitic lath are shown in Figure 9. The lath width is in the range of 100 to 600 nm, as shown in Figure 9(a). Meanwhile, the peak of the distribution curves moves to the right, indicating that the lath width decreases with increasing Mo content. The average widths of martensitic laths of the tempered steels are 362 ± 141, 277 ± 106, and 203 ± 103 nm for steel 0 pct Mo, steel 0.25 pct Mo, and steel 0.5 pct Mo, respectively. The results show that martensitic lath is also refined with increasing Mo content in steels, as shown in Figure 9(b).

With increasing Mo content, the refined blocks result in increasing the amount of HAGB. Meanwhile, the refined martensitic laths also lead to an increase of the
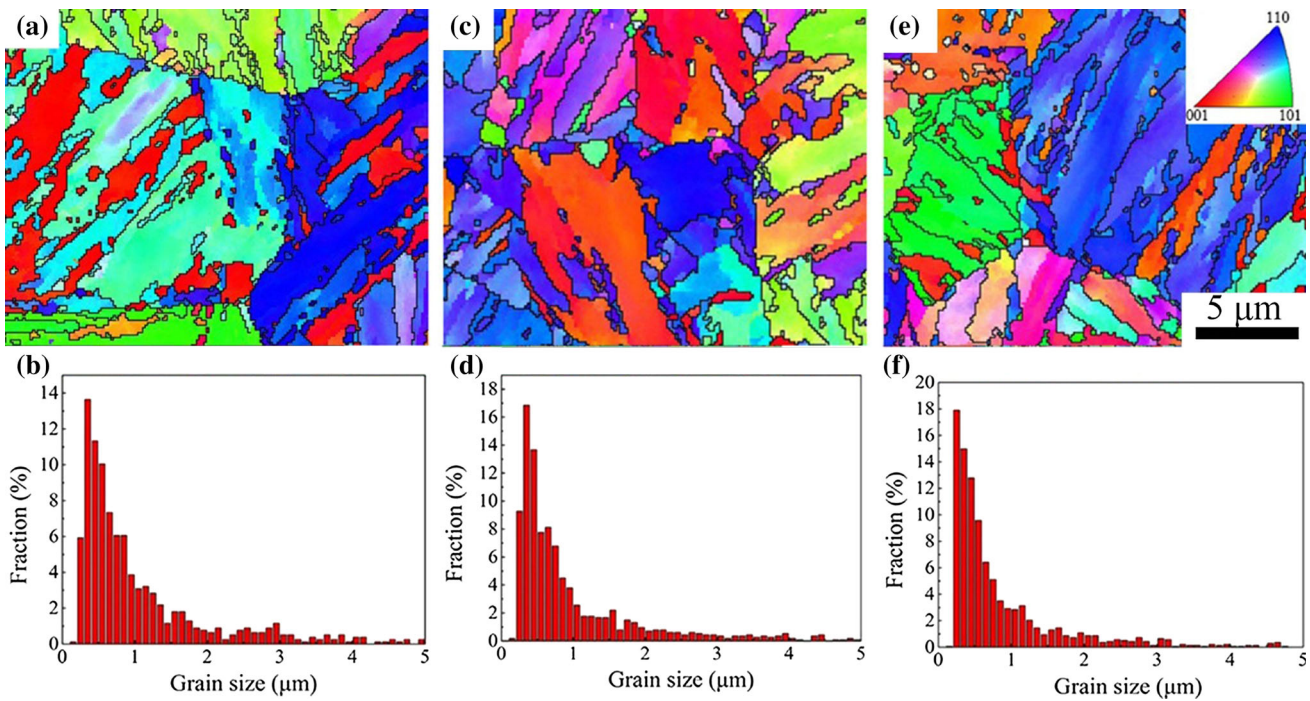

Fig. 6—Crystallographic orientation and block size distribution in the tempered steels analyzed by EBSD: (a) and (b) steel 0 pct Mo, (c) and (d) steel 0.25 pct Mo, and (e) and (f) steel 0.50 pct Mo.
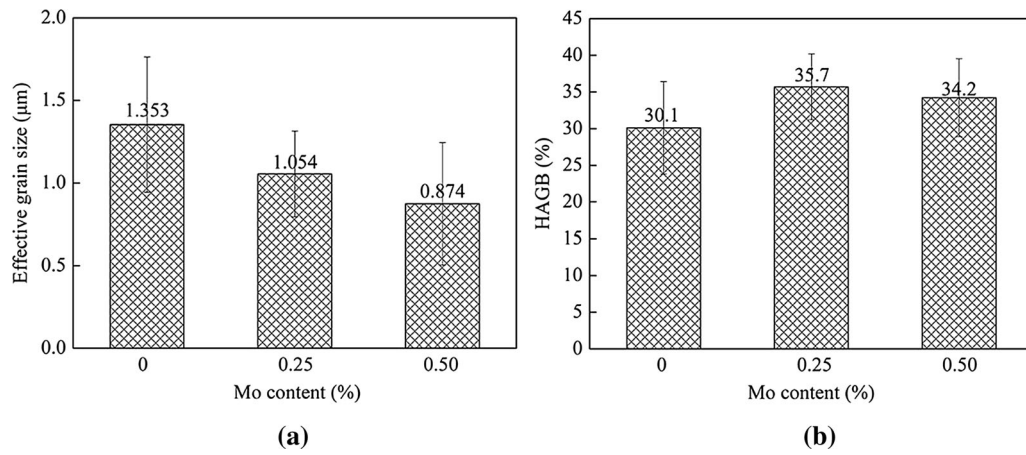
Fig. 7—Influence of Mo content on (*a*) effective grain size and (*b*) HAGB percentage.
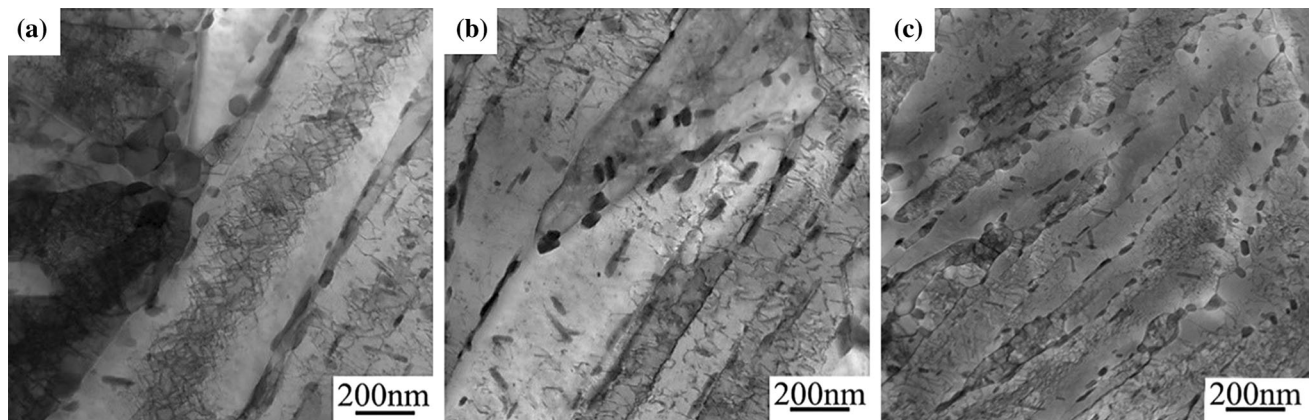

Fig. 8—Martensitic lath morphology in the tempered steels: (*a*) steel 0 pct Mo, (*b*) steel 0.25 pct Mo, and (*c*) steel 0.50 pct Mo.
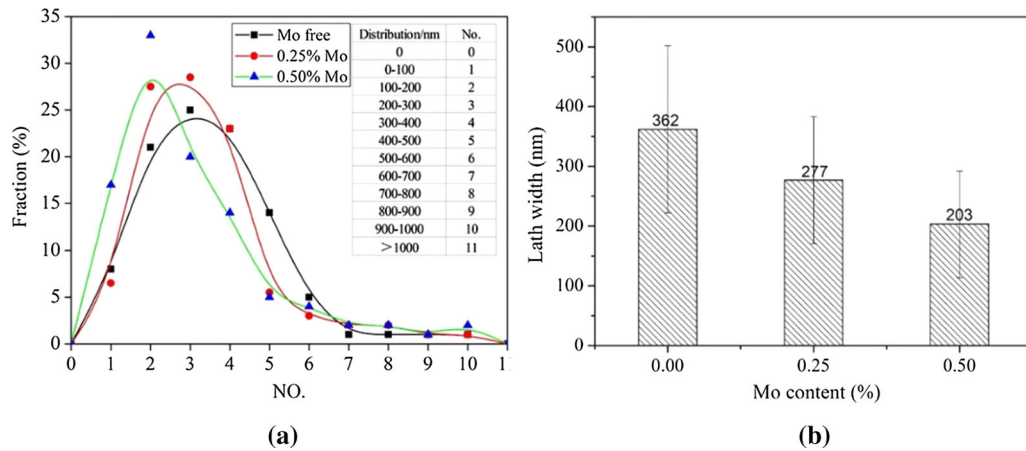

Fig. 9—(*a*) Statistical distribution of lath width and (*b*) average lath width of tested steels.

amount of LAGB. Therefore, the percentage of HAGB has no obvious change. The total amount of HAGB and LAGB increases with increasing Mo content.

In order to clarify the influence of Mo content on martensitic microstructure refinement, J Mat Pro software is used to calculate the CCT curves and phase
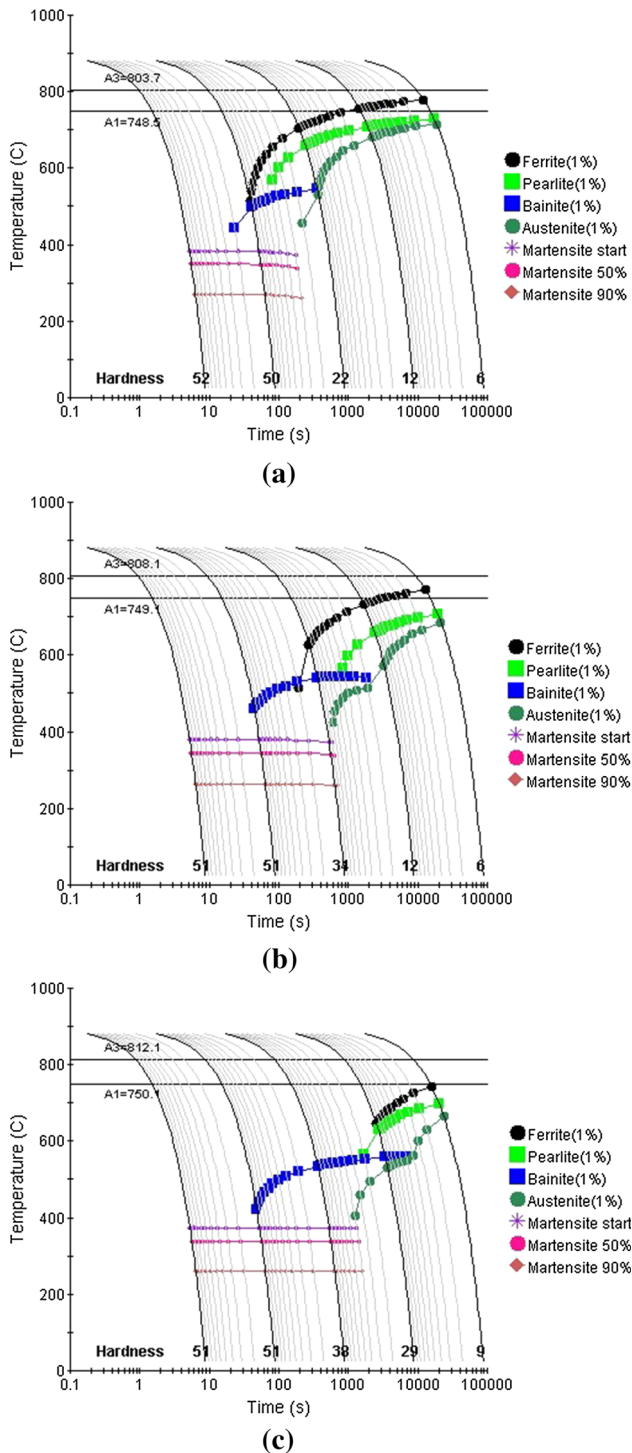
(a)

(b)

(c)

Fig. 10—CCT curves calculated by J Mat Pro software: (*a*) steel 0 pct Mo, (*b*) steel 0.25 pct Mo, and (*c*) steel 0.50 pct Mo.

transition temperatures of the steels. The CCT curves are shown in Figure 10. It is obvious that Mo delays ferrite and pearlite phase transformation. The calculation results indicate that the stability of the undercooled austenite is improved and the martensite start (M_s) temperatures decreases with increasing Mo content. Therefore, martensitic microstructure is refined.

There are many dislocations in the quenched steels, as shown in Figure 11. Dislocation density is usually characterized using XRD peak broadening.[22] The XRD detection results of the samples are shown in Figure 12. The dislocation densities are 2.48×10^{16}, 3.22×10^{16}, and 3.89×10^{16} cm^{-2} for steel 0 pct Mo, steel 0.25 pct Mo, and steel 0.5 pct Mo, respectively. The dislocation density increases obviously with increasing Mo content.

B. *Effect of Mo Content on Carbide Precipitates*

The Nb content is 0.04 pct in the experimental steels. Nb-containing particles in the quenched steel 0.5 pct Mo are observed by use of TEM, as shown in Figure 13. It was difficult to find them in the tempered sample, since there were too many carbides in that sample. Most of the Nb-containing particles are smaller than 50 nm. From the EDS result, it is found that the Nb-containing particles are similar to Nb(C, N). There is a small amount of Cr and V elements in Nb-containing particles. The Cu element comes from the copper net used for carbon extraction replica preparation.

Besides Nb-containing particles, there are many carbides in the tempered steels. The carbide morphologies, area fraction, and size distribution in the tempered steels analyzed by TEM are shown in Figures 14 and 15, respectively. The area of each carbide was measured by Image J software and the diameter of each carbide was calculated with the measured area. It is obvious that the carbides are refined and the area fraction of carbides increases with increasing Mo content in steels. The statistic analysis of carbides area fraction is based on TEM carbon extraction replica photographs. The carbide area fractions shown in Figure 15(b) are higher than the actual area fractions on the sample surface, since the samples are etched before carbon coating. Therefore, all the carbides in the volume of the etched thickness were extracted by the carbon thin film. However, the variation trend of carbide area fraction with increasing Mo content is still worthy of reference, since the etching time is the same for all samples and the etched thickness is almost the same.

The amount of carbides precipitated on dislocations also increases with increasing Mo content. It is obvious that the sizes of carbides precipitated at lath boundaries and dislocations are relatively large, as shown in Figure 16. The precipitate morphology, selected area diffraction pattern, and EDS spectrum analyzed by TEM and EDS for steel 0.50 pct Mo are shown in Figure 17. Most carbides precipitated at PAG boundaries and martensitic lath boundaries are $M_{23}C_6$, as shown in Figures 17(a) through (i). $M_{23}C_6$ carbides precipitated at PAG boundaries are spherical or elliptic and the diameter is about 100 nm, as shown in Figures 17(a) through (c). $M_{23}C_6$ carbides precipitated at lath boundaries are striplike, with diameters of 20 to 50 nm and lengths of 100 to 500 nm, as shown in Figures 17(d) through (f). $M_{23}C_6$ carbides precipitated in matrix are spherical or elliptic and their diameters are smaller than 100 nm, as shown in Figures 17(j) through (l). Most of the round bar carbides precipitated in
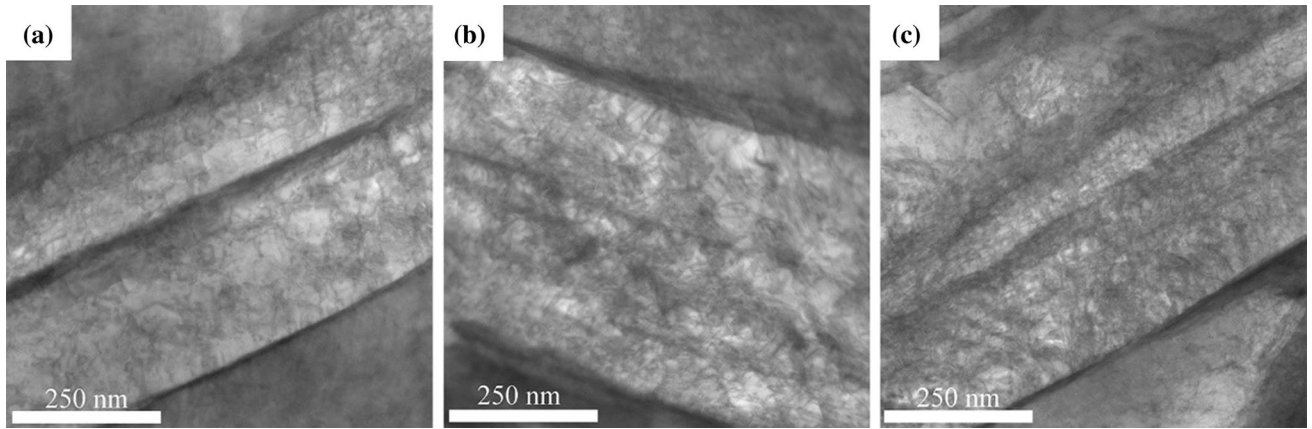
Fig. 11—Morphologies of dislocations in the quenched steels: (a) steel 0 pct Mo, (b) steel 0.25 pct Mo, and (c) steel 0.50 pct Mo.
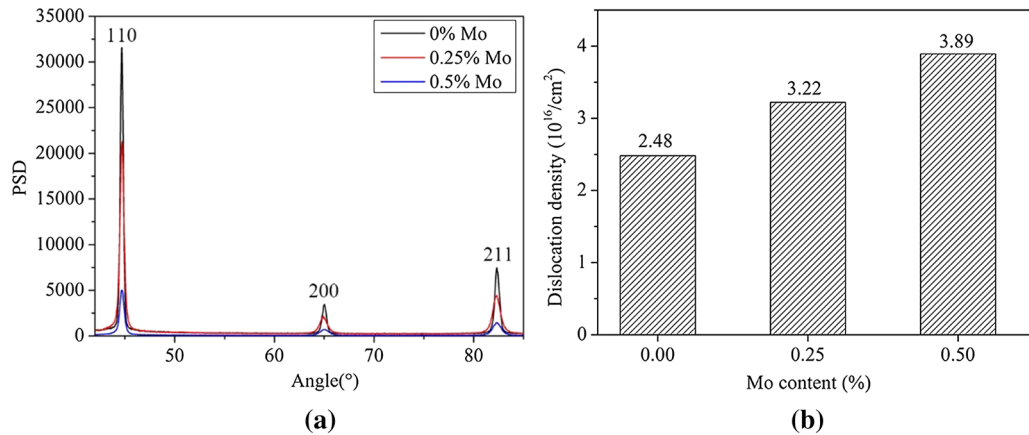

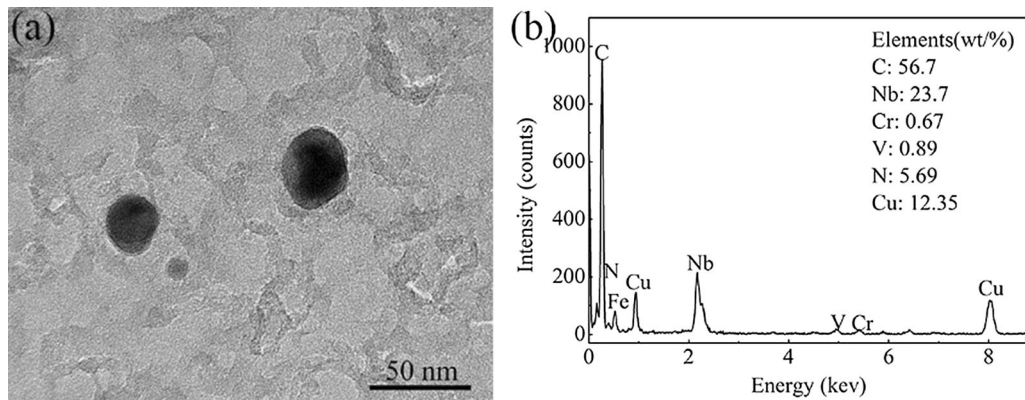Fig. 12—(a) XRD analysis result and (b) dislocation density in quenched steels.

Fig. 13—(a) Nb-containing particles morphology and (b) EDS analysis result of the quenched steel 0.5 pct Mo.

matrix are M_7C_3 and the sizes are relatively small, the diameters being smaller than 20 nm and the lengths smaller than 100 nm, as shown in Figures 17(g) through (i). The small spherical carbide precipitated in matrix is MC and the diameter is smaller than 50 nm, as shown in Figures 17(m) through (o).

The thermodynamic calculation results of the equilibrium precipitates in the tested steels are shown in Figure 18. Although the quenching and tempering heat treatment is not an equilibrium process, the calculation results on the variation of the precipitate type and quantity with Mo content in steel are worthy of
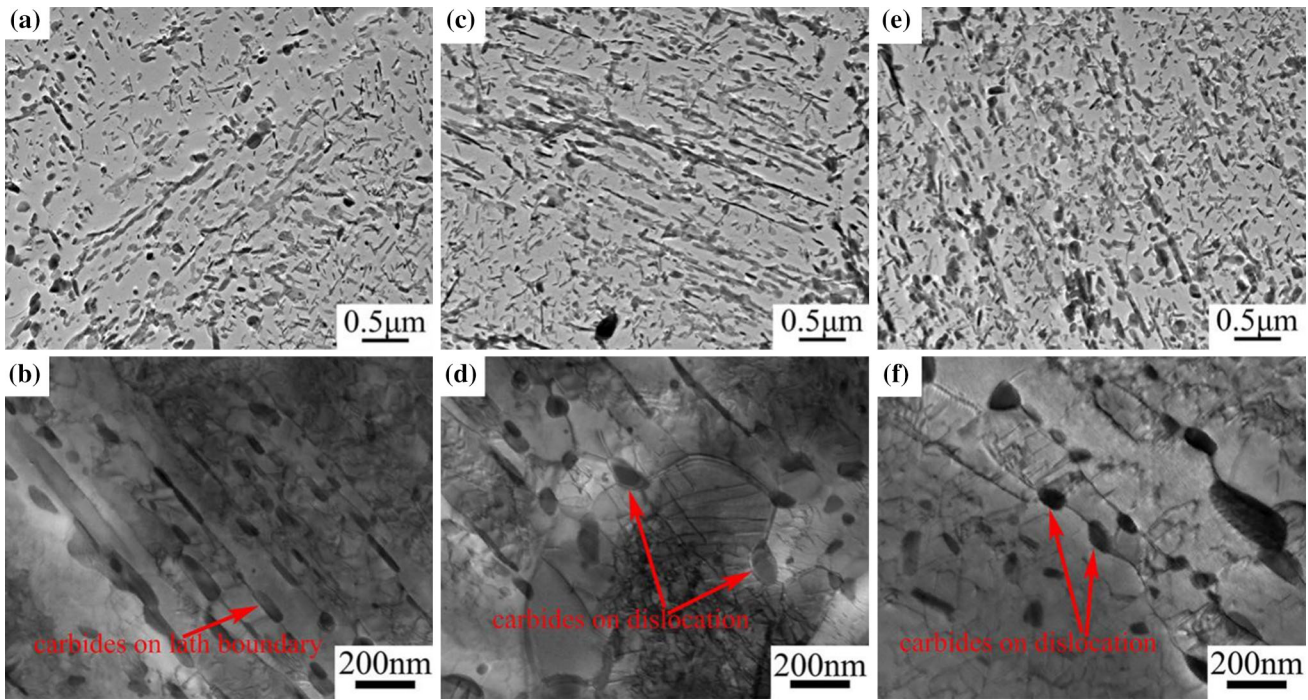
Fig. 14—Precipitate morphologies and distribution in the tempered steels: (a) and (b) steel 0 pct Mo, (c) and (d) steel 0.25 pct Mo, and (e) and (f) steel 0.50 pct Mo.
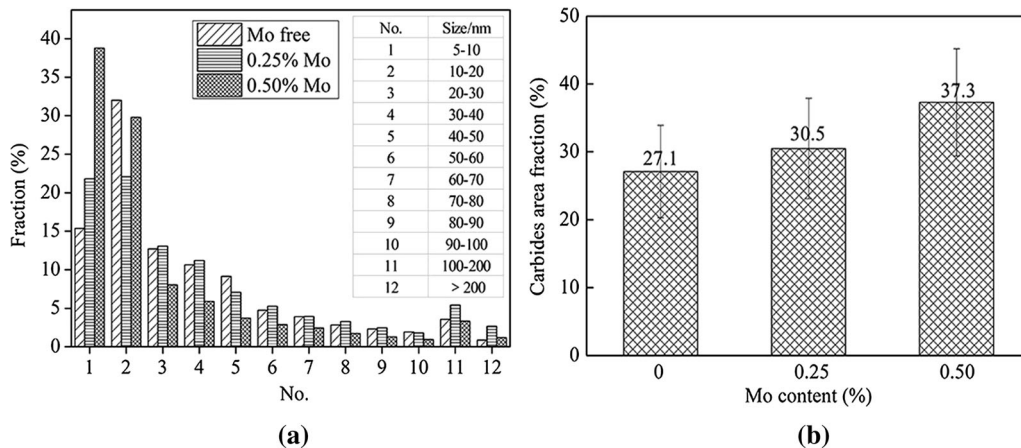

Fig. 15—(a) Carbide size distribution and (b) area fraction in tempered steels with different Mo contents.

reference. There are $M_{23}C_6$, M_7C_3, MC, cementite, fcc-A1#1(Nb(C, N)), MnS, M_2B, and BN equilibrium precipitates. $M_{23}C_6$, M_7C_3, and MC are main carbides precipitated during tempering. $M_{23}C_6$ and M_7C_3 carbides mainly contain Fe, Cr, Mo, C, and Mn elements. MC carbides are VC in Mo-free steel, while they are (Mo, V)C in Mo-bearing steels, as shown in Figure 18(f). Cementite is a kind of metastable carbide.

As shown in Table II and Figure 19, the amount of M_7C_3 carbides decreases with increasing Mo content. The amount of $M_{23}C_6$ carbides hardly changes with the addition of 0.25 pct Mo compared with Mo-free steel but increases obviously when Mo content increases from

0.25 to 0.50 pct. The precipitation amount of MC carbides increases significantly when Mo content increases from 0 to 0.25 pct and is almost the same for steel 0.25 pct Mo and steel 0.50 pct Mo. It is indicated that the addition of 0.25 pct Mo promotes the nucleation of MC. However, the precipitation of MC carbides is limited by V content and the remaining Mo atoms dissolve into $M_{23}C_6$ carbides when Mo content increases from 0.25 to 0.50 pct. Besides, a small amount of M_7C_3 carbides are transformed into $M_{23}C_6$ carbides with increasing Mo content. In addition, with increasing Mo content, the amount of cementite decreases and the temperature range of cementite becomes smaller. When
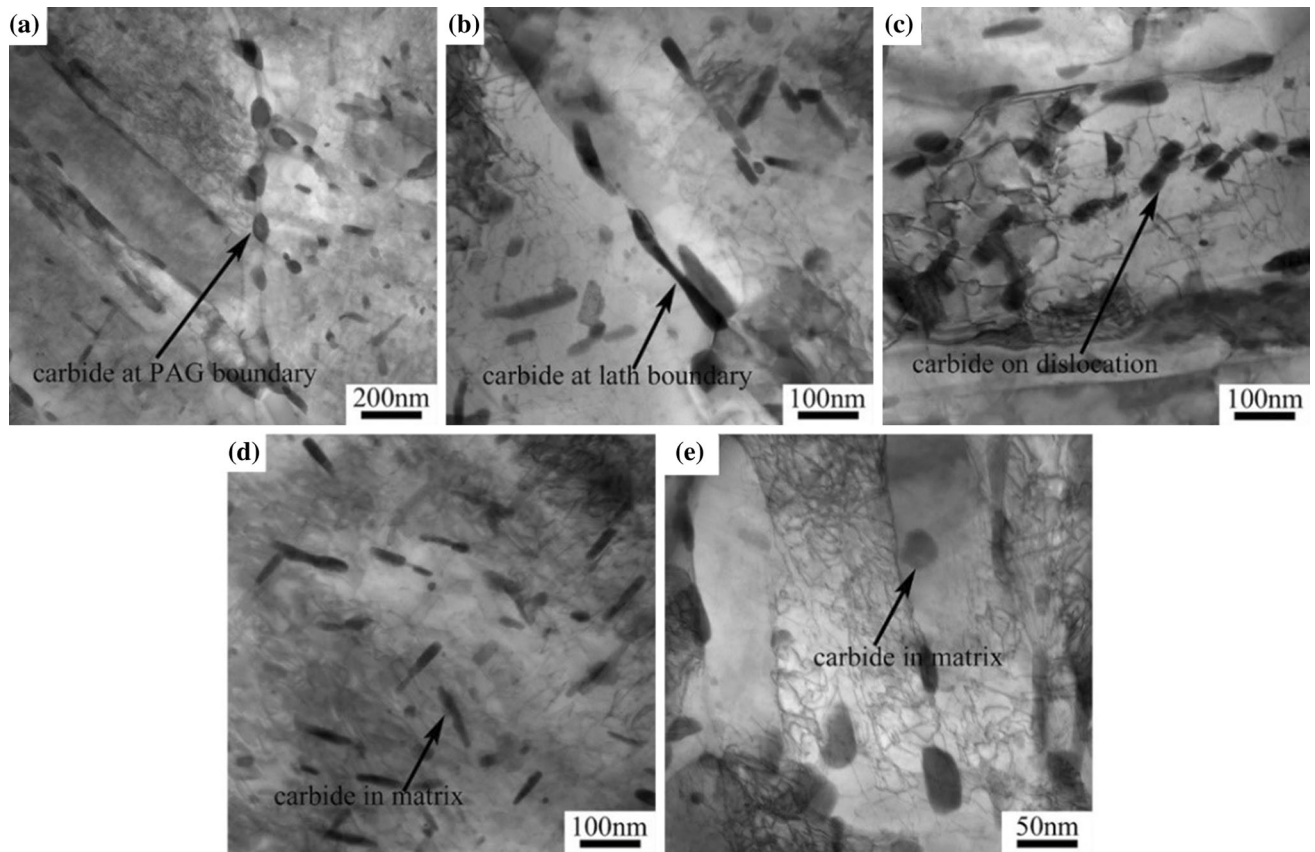
Fig. 16—Precipitate morphologies and distribution in the tempered steel 0.50 pct Mo: (*a*) carbides at PAG boundary, (*b*) carbides at lath boundary, (*c*) carbides on dislocations, and (*d*) and (*e*) carbides in matrix.

Mo content is 0.50 pct, there is almost no cementite. The striplike cementite precipitates on interlath are harmful to toughness.

The microstructure is refined, and dislocation density increases with increasing Mo content. The increment of subgrain boundaries and dislocation density accelerates the nucleation for precipitates. In addition, Mo could reduce interfacial energy and Gibbs free energy for precipitation.[4–9] Therefore, the nucleation rate of carbides increases with increasing Mo content. Mo not only accelerates precipitation of $M_{23}C_6$ carbides, but also improves their thermal stability.[23–27] The schematic diagrams of carbide distribution in the tempered steels with different Mo contents are shown in Figure 20. $M_{23}C_6$ carbides tend to precipitate at subgrain boundaries and dislocations first. Although the amount of $M_{23}C_6$ carbides increases obviously with increasing Mo content from 0.25 to 0.50 pct, there is no coarsening of $M_{23}C_6$ carbides. This is because the number of nucleation sites increases due to martensite refinement and dislocation density increment. On the other hand, the thermal stability of $M_{23}C_6$ is improved with increasing Mo fraction in carbides.

C. *Effect of Mo Content on Mechanical Properties*

The mechanical properties of the quenched and tempered steels are given in Table III. The variation of ultimate tensile strength, yield strength, and impact toughness as a function of Mo content are shown in Figure 21. The ultimate tensile strength and yield strength increase by about 160 MPa with the addition of 0.50 pct Mo. Hardness increases by HRC 4.3 with the addition of 0.25 pct Mo compared with steel 0 pct Mo but remains constant when Mo content increases from 0.25 to 0.50 pct. The impact toughness, elongation, and reduction of area all vary in a similar way with increasing Mo content. They decrease slightly with the addition of 0.25 pct Mo, while there is no obvious change with an increase in the Mo content from 0.25 to 0.50 pct in the studied steels.

The impact fracture morphologies for the steels with different Mo contents are shown in Figure 22. The photos in the upper right corner of Figures 22(a) through (c) show the low-magnification fracture morphologies. There are no macrocracks on these fractures. There are many small dimples on the fracture surfaces, as shown in Figures 22(d) through (f). In addition, there
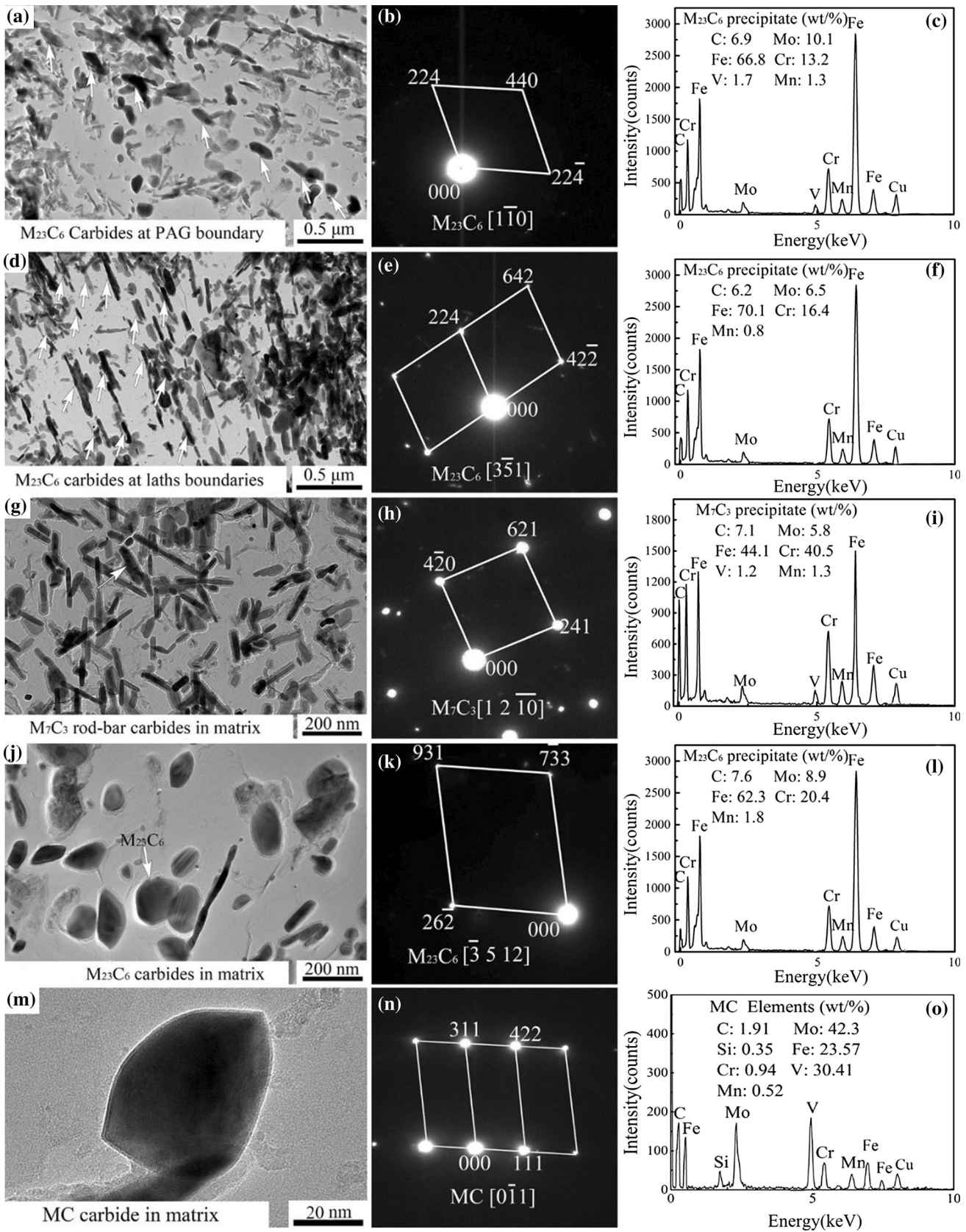
Fig. 17—Precipitate morphologies and types in the tempered steel 0.50 pct Mo: (*a*) through (*c*) $M_{23}C_6$ carbides precipitated at PAG boundary, (*d*) through (*f*) $M_{23}C_6$ carbides precipitated at lath boundary, (*g*) through (*i*) M_7C_3 carbides precipitated in matrix, (*j*) through (*l*) $M_{23}C_6$ carbides precipitated in matrix, and (*m*) through (*o*) MC carbides precipitated in matrix.
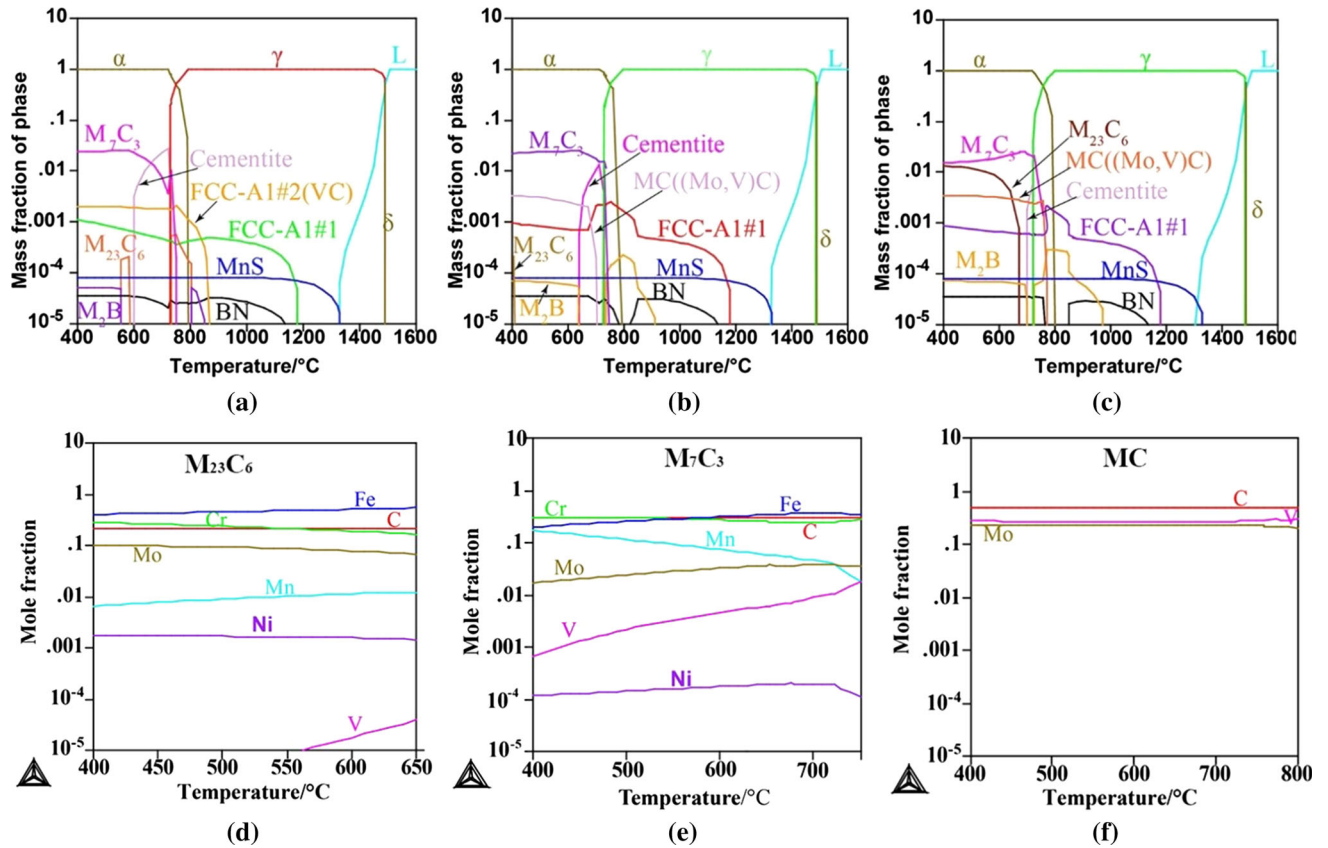
Fig. 18—Thermodynamic calculation results: (*a*) steel 0 pct Mo, (*b*) steel 0.25 pct Mo, and (*c*) steel 0.50 pct Mo; (*d*), (*e*), and (*f*) chemical compositions of $M_{23}C_6$, M_7C_3, and MC, respectively, in steel 0.50 pct Mo.

Table II. Mass Fractions of Precipitates in the Experimental Steels Calculated by Thermo-Calc

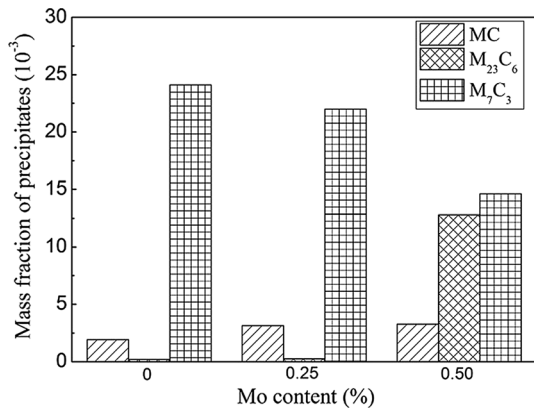| Steel	Mo (Pct)	Fcc_A1#1(Nb(C,N))	MC	M_7C_3	$M_{23}C_6$	BN	M_2B
1	0	1.06×10^{-3}	1.91×10^{-3}	2.41×10^{-2}	1.89×10^{-4}	3.39×10^{-5}	4.87×10^{-5}
2	0.25	9.24×10^{-4}	3.14×10^{-3}	2.20×10^{-2}	2.43×10^{-4}	3.39×10^{-5}	6.68×10^{-5}
3	0.50	9.00×10^{-4}	3.28×10^{-3}	1.46×10^{-2}	1.28×10^{-2}	3.39×10^{-5}	6.99×10^{-5}

Fig. 19—Variation of mass fractions of carbides with different Mo contents calculated by Thermo-Calc.

are some tear ridges, indicating that there was a considerable degree of plastic deformation before fracture. Therefore, the impact fracture modes of the experimental steels are ductile.

Since the steels are used for train axle, the rotating-bending fatigue test was conducted to evaluate the safety of the axle material. The fatigue strengths are 543, 577, and 617 MPa for steel 0 pct Mo, steel 0.25 pct Mo, and steel 0.5 pct Mo, respectively, as shown in Table III. The variation trend of fatigue strength is the same as that of ultimate tensile strength, which is improved with increasing Mo content in steel. The tests of S-N curves of steel 0 pct Mo and steel 0.5 pct Mo are conducted due to the significant difference of the fatigue strength between these two tested steels. The results show that the fatigue property of steel 0.5 pct Mo is obviously better than that of steel 0 pct Mo, as shown in
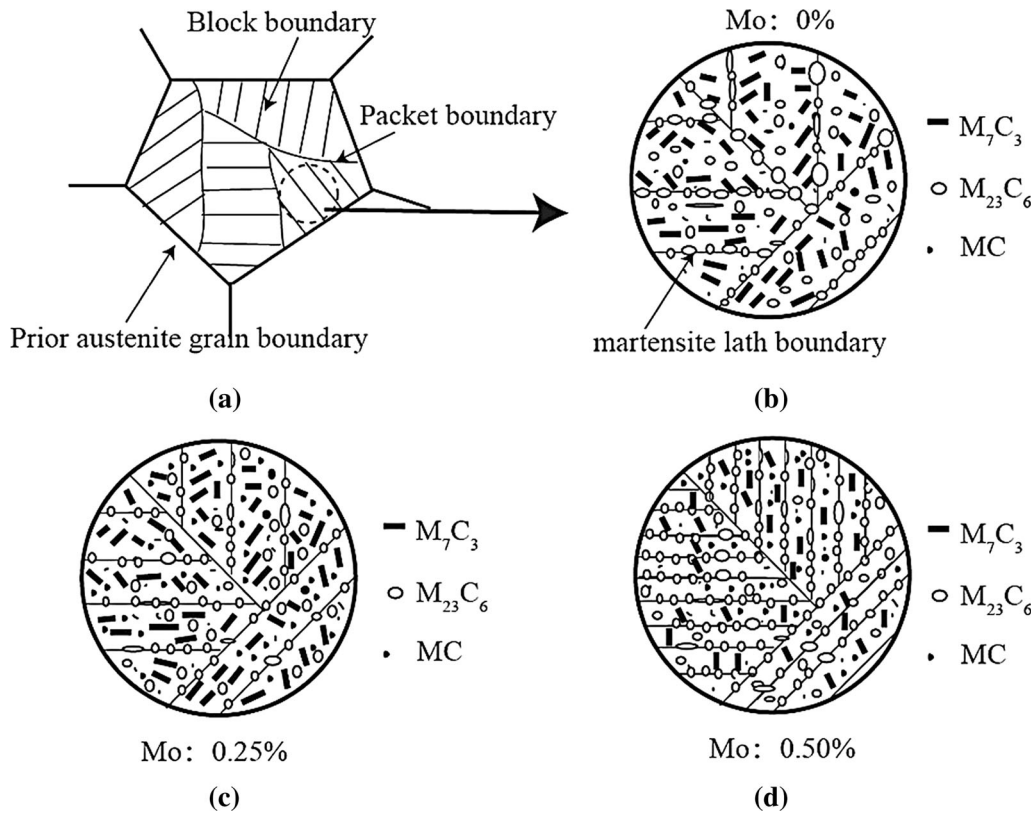
Fig. 20—Schematic diagram of carbide distribution in the tempered steels with different Mo contents: (*a*) schematic diagram of martensite structure, (*b*) carbide precipitation in steel 0 pct Mo, (*c*) carbide precipitation in steel 0.25 pct Mo, and (*d*) carbide precipitation in steel 0.50 pct Mo.

Figure 23. The values of elongation are 18.4, 17.2, and 17.4 pct and those of reduction of area are 55.2, 52.6, and 52.5 pct for steel 0 pct Mo, steel 0.25 pct Mo, and steel 0.5 pct Mo, respectively, as shown in Table III. Therefore, the experimental steels are ductile material. Hosford[28] reported that the softer, more ductile material would have longer life at high strain amplitudes (low-cycle fatigue), whereas the stronger, higher strength, and less ductile material would have longer life at low strain amplitudes (high-cycle fatigue). This suggests that for good low-cycle fatigue, one would want a material with a high true strain to fracture, which is a very ductile material. For good high-cycle fatigue, one would want a very high strength material. Assuming that a very ductile material would have low strength and a very high strength material would have low ductility, where we would use the low strength material if low-cycle fatigue was the concern and we would use a very high strength material if good high-cycle fatigue resistance was desired. From the mechanical properties in Table III, it can be seen that the steel 0.5 pct Mo not only has high strength but also has good ductility, which has excellent fatigue strength of 617 MPa when the fatigue life is more than 10^7 cycles. Meanwhile, it also has a high true strain to fracture when the fatigue life is less than 10^7 cycles.

The overall views of the fracture surface of steel 0 pct Mo with stress of 560 MPa and rotating cycles of 220,251 and steel 0.5 pct Mo with stress of 640 MPa and rotating cycles of 195,291 are shown in Figures 24(a) and (b), respectively. Normally, the fracture surface is composed of the crack initiation region, crack propagation region, and final fracture region.[29] The crack initiation regions are marked with white arrows and the crack propagation regions with dotted black lines. Magnified views of the crack initiation region A, crack propagation region B, transition region C, and final fracture region D in Figure 24(b) are shown in Figures 25(a), (b), (c), and (d), respectively. The crack initiation regions are near the surface of the sample and no inclusion is detected, which indicates that the fatigue cracks are not initiated by inclusions. Fatigue marks are observed in the crack propagation region, as shown in Figure 25(b). There are many small dimples in the transition region between the crack propagation region and the final fracture region, as shown in Figure 25(c), which indicates that there is plastic deformation before fracture. However, the final fracture surface is cleavage, as shown in Figure 25(d). Inclusions are observed in crack propagation regions on the fracture surfaces, as shown in Figure 26. The size of inclusions is 5 to 10 μm, and there are fatigue marks around the inclusions.

Table III.   Mechanical Properties of the Experimental Steels

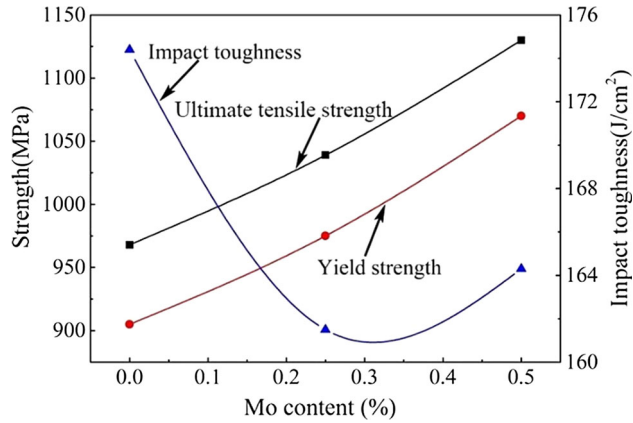| Steel	Mo (Pct)	Impact Toughness (J/cm²)	Ultimate Tensile Strength (MPa)	Yield Strength (MPa)	Hardness (HRC)	Elongation (Pct)	Reduction of Area (Pct)	Fatigue Strength (MPa)
1	0	174.4 ± 6.3	968 ± 16.4	905 ± 15.2	31.3 ± 1.2	18.4 ± 0.4	55.2 ± 1.3	543
2	0.25	161.5 ± 5.8	1039 ± 21.1	975 ± 16.5	35.6 ± 0.7	17.1 ± 0.5	52.6 ± 1.1	577
3	0.50	164.3 ± 6.0	1130 ± 18.7	1070 ± 20.3	36.0 ± 0.8	17.4 ± 0.4	52.5 ± 1.3	617

Fig. 21—Variations of strength and impact toughness with increasing Mo content.
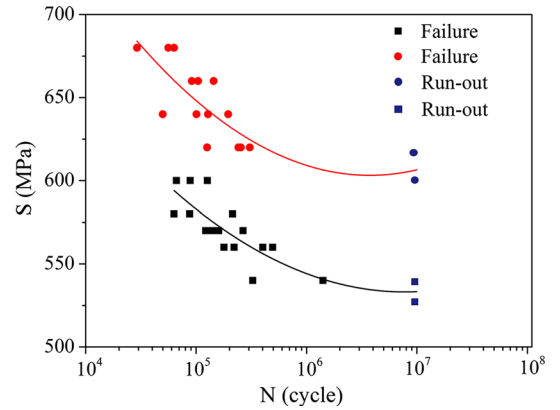

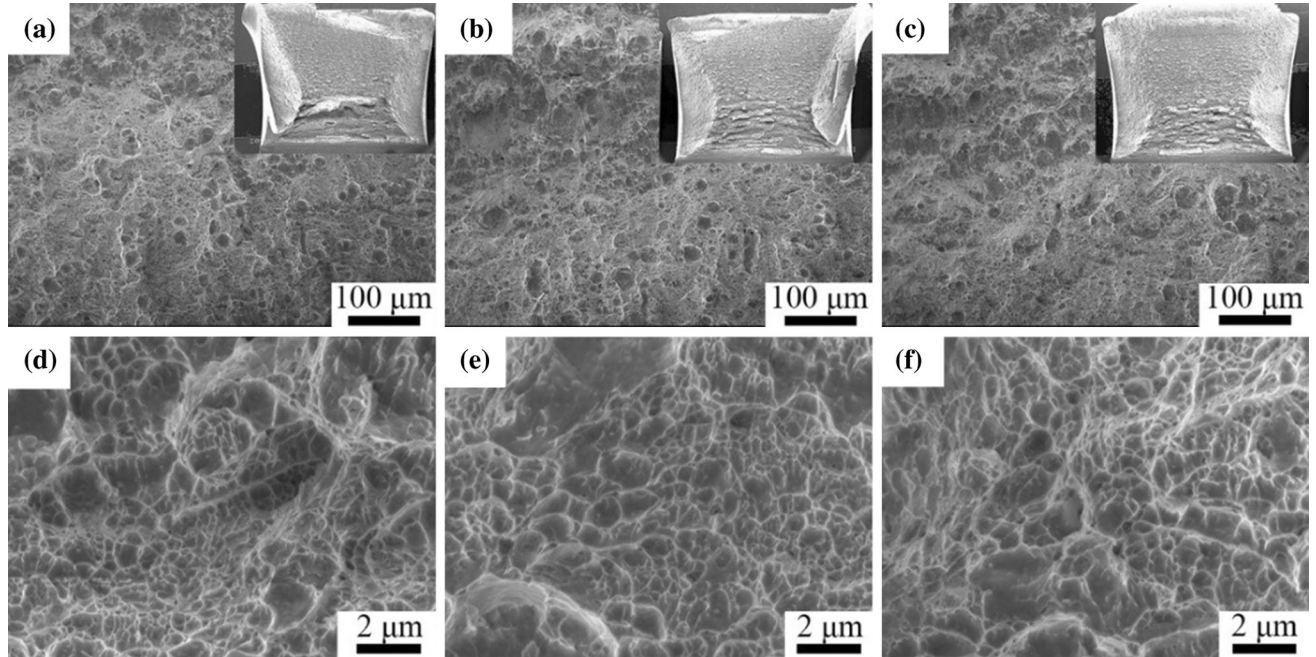Fig. 23—S-N curves of rotating-bending fatigue testing.

Fig. 22—Impact fracture morphologies: (*a*) and (*d*) steel 0 pct Mo, (*b*) and (*e*) steel 0.25 pct Mo, and (*c*) and (*f*) steel 0.50 pct Mo.
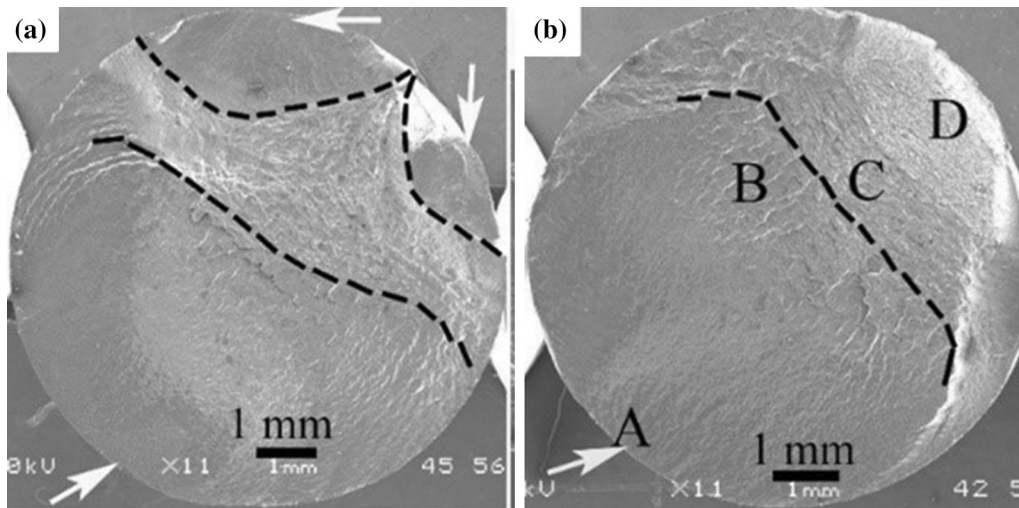
Fig. 24—Overview of fatigue fracture surfaces: (*a*) steel 0 pct Mo and (*b*) steel 0.5 pct Mo.
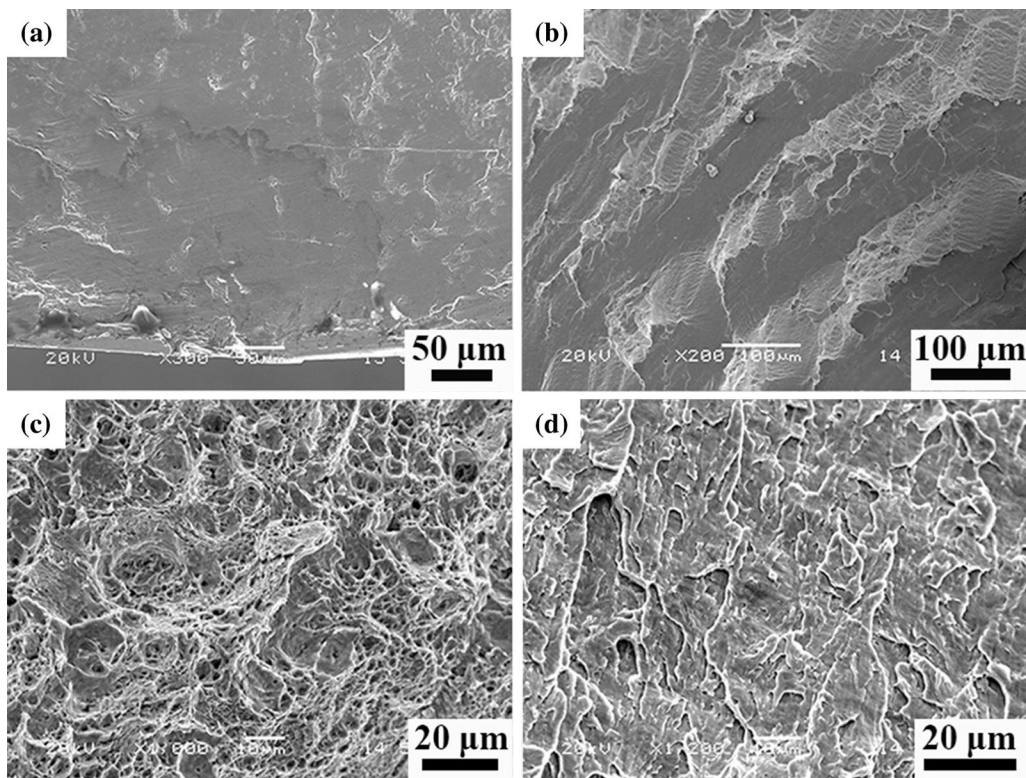

Fig. 25—Magnified view of the fatigue fracture surfaces of Fig. 24(b): (*a*) crack initiation region A, (*b*) crack propagation region B, (*c*) transition region C, and (*d*) final fracture region D.

The ultimate tensile strength and yield strength increase with increasing Mo content in the studied steels. With increasing Mo content in the experimental steels, the block size decreases and the block boundaries increase. The block boundary is the most effective grain boundary for strength in lath martensite, since the block boundary significantly restricts the motion of dislocations.[30–33] The martensitic lath width is also refined with increasing Mo content. The lath boundaries can also act as barriers to dislocation motion and have a strengthening effect.[33,34] In addition, the amount of MC carbide whose size is smaller than 50 nm increases with the addition of 0.25 pct Mo. The precipitation strengthening effect resulting from small size MC carbides is improved. With increasing Mo contents from 0.25 to 0.50 pct, the amount of $M_{23}C_6$ carbides increases and the size is relatively smaller than the carbides in lower Mo content steels. The precipitation
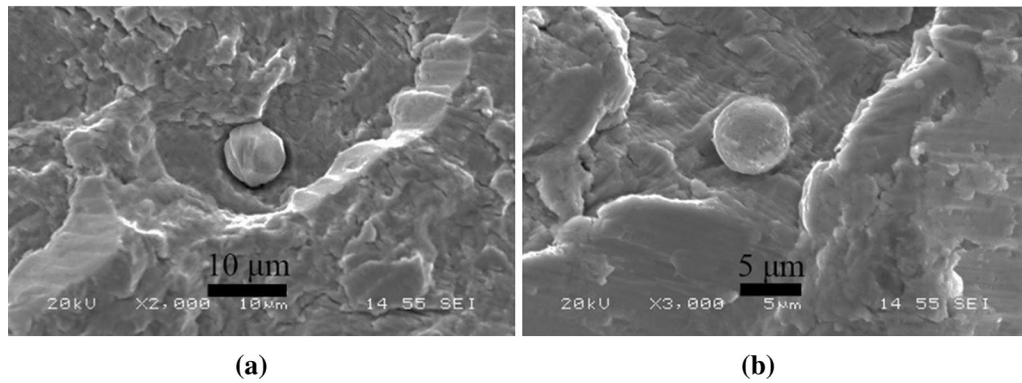
(wt/%) Al: 45.01 Ca: 1.46 Mg: 5.45 O: 38.37

(wt/%) Al: 10.25 Ca: 2.02 Si: 27.5 O: 44.34

(a)   **(b)**

Fig. 26—Inclusions in the crack propagation region of fatigue fracture surfaces: (*a*) steel 0 pct Mo and (*b*) steel 0.5 pct Mo.

strengthening effect of the steel material is inversely proportional to the average spacing of particles or the f/r (f is the particle volume fraction and r is the particle radius). Therefore, refining the carbide precipitates and decreasing the distance between carbides can improve strength. Besides, the carbides precipitated at martensitic lath boundaries and dislocations have a strengthening effect and can suppress the coarsening of martensitic lath and the movement of dislocations during tempering. Therefore, the strength is improved.

The impact toughness decreases with the addition of 0.25 pct Mo, and there is no obvious change with further increasing Mo content from 0.25 to 0.50 pct in the experimental steels. According to Thermo-Calc calculation, the amount of MC carbides increases with the addition of 0.25 pct Mo. The small size MC carbides precipitated in matrix can reduce impact toughness, since the precipitation strengthening deteriorates toughness due to the pinning effect of fine particles on dislocations. When Mo content is increased from 0.25 to 0.50 pct, although the precipitation of $M_{23}C_6$ carbides increases, there is no coarsening of $M_{23}C_6$ carbides. This is because the number of nucleation sites is increased and the thermal stability of $M_{23}C_6$ is improved with increasing Mo fraction in carbides. In addition, the size of $M_{23}C_6$ carbides is relatively larger than that of MC carbides and the pining effect on dislocations is weaker than MC carbides. Therefore, the adverse effect on toughness resulting from $M_{23}C_6$ carbides is relatively weaker than MC carbides.

The refined blocks are beneficial for improving toughness.[19–21] The refined martensitic laths are also beneficial for obtaining ductility fracture and improving toughness.[35] Therefore, although the tensile strength is improved, the impact toughness is not deteriorated by the addition of 0.50 pct Mo compared with the 0.25 pct Mo in steel. Meanwhile, the fatigue strength is significantly improved with the addition of 0.50 pct Mo. The fatigue crack initiation is dominated by the strength of the experimental material, while the crack propagation is controlled by toughness. The fatigue strengths of the experimental steels are improved with increasing the ultimate tensile strength when the toughness is at the

same level, since the fatigue crack initiation on the specimen surface becomes more difficult with increasing material strength.

IV. CONCLUSIONS

In this article, the effects of Mo contents of 0.25 and 0.50 pct on refining martensitic microstructure and carbide precipitates were studied. The effects of martensitic structure and dislocation density on carbide precipitation behavior in the tempered steels were also analyzed. Meanwhile, the comprehensive effects of martensitic structure and carbide precipitates on mechanical properties were discussed. The conclusions are as follows.

1. With the addition of Mo contents of 0.25 and 0.50 pct in the experimental steels, the martensitic blocks and laths are refined due to decreasing the M_s temperature. Meanwhile, the dislocation density increases with increasing Mo content.
2. Most of the carbides precipitated at PAG boundaries and subgrain boundaries are $M_{23}C_6$, whose size is relatively large. M_7C_3 and MC carbides precipitate in matrix and their sizes are relatively small. Thermo-Calc calculation results show that the amount of MC carbides increases with an addition of 0.25 pct Mo and the amount of $M_{23}C_6$ carbides increases with increasing Mo content from 0.25 to 0.50 pct.
3. The carbides are refined and the amount of carbides increases with increasing Mo content up to 0.50 pct in the studied steels due to the increment of carbide nucleation sites resulting from martensitic structure refinement and dislocation density increment. Besides, the improvement of thermal stability of $M_{23}C_6$ carbides enriched with Mo also contributes to carbide refinement.
4. The ultimate tensile strength is improved and the impact toughness is not deteriorated with the addition of 0.50 pct Mo compared with the steel 0.25 pct Mo due to the refinement of martensitic structure and carbides. The fatigue strength is

significantly improved with the addition of 0.50 pct Mo.

REFERENCES

1. J. Dong, X. Zhou, Y. Liu, C. Li, C. Liu, and Q. Guo: *Mater. Sci. Eng. A*, 2017, vol. 683, pp. 215–26.
2. J. Kong, L. Zhen, B. Guo, P. Li, A. Wang, and C. Xie: *Mater. Des.*, 2004, vol. 25, pp. 723–28.
3. W. Lee, S. Hong, C. Park, K. Kim, and S. Park: *Scripta Mater.*, 2000, vol. 43, pp. 319–24.
4. L. Cheng, Q. Cai, B. Xie, N. Zhen, X. Zhou, and G. Li: *Mater. Sci. Eng. A*, 2016, vol. 651, pp. 185–91.
5. Y.W. Kim, J.H. Kim, S.G. Hong, and C.S. Lee: *Mater. Sci. Eng. A*, 2014, vol. 605, pp. 244–52.
6. Z. Wang, X. Sun, Z. Yang, Q. Yong, C. Zhang, Z. Li, and Y. Weng: *Mater. Sci. Eng. A*, 2013, vol. 573, pp. 84–91.
7. C. Chen, H. Yen, F. Kao, W. Li, C. Huang, and J. Yang: *Mater. Sci. Eng. A*, 2009, vol. 499, pp. 162–66.
8. C. Chen, C. Chen, and J. Yang: *Mater. Charact.*, 2014, vol. 88, pp. 69–79.
9. Z. Zhang, Q. Yong, X. Sun, Z. Li, J. Kang, and G. Wang: *J. Iron Steel Res. Int.*, 2015, vol. 22, pp. 337–43.
10. S.P. Hong, S.I. Kim, T.Y. Ahn, S.T. Hong, and Y.W. Kim: *Mater. Charact.*, 2016, vol. 115, pp. 8–13.
11. K. Maruyama, K. Sawada, and J. Koike: *ISIJ Int.*, 2001, vol. 41, pp. 641–53.
12. R. Uemori, R. Chijiiwa, H. Tamehiro, and H. Morlkawa: *Appl. Surf. Sci.*, 1994, vol. 76, pp. 255–60.
13. K. Wieczerzak, P. Bala, M. Stepien, G. Cios, and T. Koziel: *Mater. Des.*, 2016, vol. 94, pp. 61–68.
14. T. Wada and W.C. Hagel: *Metall. Mater. Trans. A*, 1976, vol. 7A, pp. 1419–26.
15. Y. Zheng, F. Wang, C. Li, and Y. He: *Mater. Sci. Eng. A*, 2017, vol. 701, pp. 45–55.
16. Y. Zheng, F. Wang, C. Li, Y. Li, and J. Cheng: *Mater. Sci. Eng. A*, 2018, vol. 712, pp. 453–65.
17. C. Wang, M. Wang, J. Shi, W. Hui, and H. Dong: *Scripta Mater.*, 2008, vol. 58, pp. 492–95.
18. P. Yan, Z. Liu, H. Bao, Y. Weng, and W. Liu: *Mater. Des.*, 2014, vol. 54, pp. 874–79.
19. C. Zhang, Q. Wang, J. Kong, G. Xie, M. Wang, and F. Zhang: *J. Iron Steel Res. Int.*, 2013, vol. 20, pp. 62–67.
20. Z. Luo, J. Shen, S. Hang, Y. Ding, C. Yang, and Z. Xing: *J. Iron Steel Res. Int.*, 2010, vol. 17, pp. 40–48.
21. J.W. Morris, Jr: *ISIJ Int.*, 2011, vol. 51, pp. 1569–75.
22. F. HajyAkbary, J. Sietsma, A.J. Böttger, and M.J. Santofimia: *Mater. Sci. Eng. A*, 2015, vol. 639, pp. 208–18.
23. Z. Zhang, X. Sun, Q. Yong, Z. Li, Z. Wang, and G. Wang: *Acta Metall. Sinica*, 2016, vol. 52, pp. 410–18.
24. Z. Zhang, X. Sun, Q. Yong, Z. Li, Z. Wang, and G. Wang: *Acta Metall. Sinica*, 2015, vol. 51, pp. 315–24.
25. F. Abe: *Sci. Technol. Adv. Mater.*, 2008, vol. 9, pp. 1–15.
26. P. Michauda, D. Delagnesa, P. Lamesle, M.H. Mathon, and C. Levaillant: *Acta Mater.*, 2007, vol. 55, pp. 4877–89.
27. Z. Wang, H. Zhang, C. Guo, W. Liu, Z. Yang, X. Sun, Z. Zhang, and F. Jiang: *J. Mater. Sci.*, 2016, vol. 51, pp. 4996–5007.
28. W.F. Hosford: *Mechanical Behavior of Materials*, 2nd ed., Cambridge University Press, New York, NY, 2010, pp. 281–332.
29. P. Verma, N.C.S. Srinivas, and V. Singh: *Mater. Sci. Eng. A*, 2018, vol. 715, pp. 17–24.
30. S. Morito, H. Yoshida, T. Maki, and X. Huang: *Mater. Sci. Eng. A*, 2006, vol. 438, pp. 237–40.
31. A. Shibata, T. Nagoshi, M. Sone, S. Morito, and Y. Higo: *Mater. Sci. Eng. A*, 2010, vol. 527, pp. 7538–44.
32. Y. Mine, K. Hirashita, H. Takashima, M. Matsuda, and K. Takashima: *Mater. Sci. Eng. A*, 2013, vol. 560, pp. 535–44.
33. C. Du, J. Hoefnagels, R. Vaes, and M. Geers: *Scripta Mater.*, 2016, vol. 116, pp. 117–21.
34. K. Kwak, T. Mayama, Y. Mine, and K. Takashima: *Mater. Sci. Eng. A*, 2016, vol. 674, pp. 104–16.
35. Y. Liang, S. Long, P. Xu, Y. Lu, Y. Jiang, Y. Liang, and M. Yang: *Mater. Sci. Eng. A*, 2017, vol. 695, pp. 154–64.